

## Supplementary information:

# “Additive Engineering in $\text{CH}_3\text{NH}_3\text{PbBr}_3$ Single Crystals for Terahertz Devices and Tunable High Order Harmonics”

*Sarvani Jowhar Khanam<sup>a</sup>, Srinivasa Rao Konda<sup>b,#</sup>, Azmeera Premalatha<sup>a</sup>, Ravi Ketavath<sup>a</sup>, Wufeng Fu<sup>b</sup>, Wei Li<sup>b,†</sup>, and Murali Banavoth<sup>a,\*</sup>*

*<sup>a</sup>Solar Cells and Photonics Research Laboratory, School of Chemistry, University of Hyderabad, Hyderabad 500046, Telangana, India*

*<sup>b</sup>GPL, State Key Laboratory of Applied Optics, Changchun Institute of Optics, Fine Mechanics and Physics, Chinese Academy of Sciences, Changchun, 130033, China*

*corresponding authors: \* [murali.banavoth@uohyd.ac.in](mailto:murali.banavoth@uohyd.ac.in), # [ksrao@ciomp.ac.cn](mailto:ksrao@ciomp.ac.cn),*

*† [weili1@ciomp.ac.cn](mailto:weili1@ciomp.ac.cn)*

### **1. Materials and Methods:**

#### ***1.1. Synthesis of $\text{MAPbBr}_3$ Crystals Growth with additives:***

We used additives to grow methylammonium lead bromide ( $\text{MAPbBr}_3$ ) [hereafter abbreviated as MA] crystals to investigate the impact of different ammonium salts as an additive on optoelectronic and structural properties. Ammonium salts used are aliphatic, aromatic, and chiral additives to see the effect on HHG studies. Aliphatic like Choline bromide (CB), aromatic additives like Phenylethylamine hydrochloride (PEA), P-Xylylenediamine (PXA), and chiral additives like (R)3-Aminopiperidine dihydrochloride (API).

**1.1.1 Chemicals:** Lead bromide ( $\geq 98\%$ ), methylammonium bromide (99.9% trace metals basis), dimethylformamide (DMF) (HPLC, 99.8%), and dimethyl sulfoxide (DMSO) (anhydrous,  $\geq 99.9\%$ ), were purchased from Sigma-Aldrich. Phenylethylamine hydrochloride (PEA), (R)3-aminopiperidine dihydrochloride (API), P-xylylene diamine (PXA), and choline bromide (CB) were purchased from TCI and used as received.

**1.1.2 Synthesis:** Optimal volume ratios of the solvents are prepared by dissolving the MABr, PbBr<sub>2</sub>, with 1:1 equivalents labelled it as precursor solution (MA crystal without additive for comparison) by following the previous literature in the glove box.<sup>1</sup> We have optimized the percentage of additives (A) from 0.1 to 0.2 equivalents in precursor solution for MA-A crystal growth. For example, we grow MA-API crystal by adding an optimal percentage of API to precursor solution. The precursor solution was then kept for stirring for eight hours and filtered through a polytetrafluoroethylene (PTFE) filter with 0.45  $\mu\text{m}$  pore size. Initially, tiny perovskite crystals with an average length of 1.5 mm, were obtained, which were used as seed crystals for growing larger crystals. Further, a larger crystal was achieved by carefully transferring seed crystals to the freshly prepared 1M precursors solution. We observed a possible shape control of the crystal by the geometry of crystals using the additive. Finally, add the dichloromethane (DCM) to the crystals after removing the precursor solution using the syringe; a white residue will appear on the surface of the crystals need to add; the DMF for clean the excess unreacted material from the surface. Repeat the same procedure until the solution becomes colourless when adding DCM.<sup>2</sup> Finally, perovskite SCs were dried in a vacuum oven and stored in the desiccator. The thickness of the SCs are measured using the digital vernier callipers, and MA, MA-CB, MA-PEA, MA-PXA and MA-API have a thickness of 1.02, 1.18, 1.12, 1.10, 1.03 mm, respectively.

## 1.2. Experimental device

**UV-Vis Spectra:** The absorption spectra were obtained using a UV–vis spectrometer (UV-2600 of SHIMADZU) with an integrating sphere.

**Photoluminescence Spectroscopy:** Photoluminescence (PL) spectra recorded with a Confocal Raman Microscope (Model: Witec-Alpha300) using 405 and 488 nm laser and for 800 nm wavelength Ti: Sapphire (Spectra-Physics) laser pulses of 35 fs and 1 kHz repetition rate were used.

**TRPL- Lifetime Measurements** Photoluminescence (PL) decays and PL lifetime has been recorded on a time-resolved Micro-Time 200 confocal fluorescence lifetime imaging microscopy (FLIM) setup (PicoQuant) equipped with an inverted microscope (Olympus IX 71) using laser 370.

**Confocal Raman Images:** Confocal Raman Images were taken with a Confocal Raman Microscope (Model: Witec-Alpha300)

SEM images are taken using the ZEISS field-emission scanning electron microscope (FESEM).

**X-ray Photoelectron Spectroscopy (XPS):** surface elementals mapping of crystals has been done using Thermo Fisher Scientific Pvt. Ltd, X-ray Photoelectron Spectroscopy.

**Powder XRD spectra:** The structural studies have been analyzed by a PAN-alytical xpert3 powder diffractometer with Cu K $\alpha$  radiation and the step size of 0.016711° with 73.025 times per step in ambient conditions.

**Single crystal XRD:** The X-ray crystal data of the MA and Modified MA PSCs were collected on an Xtlab Synergy Rigaku oxford diffraction with HyPix- 3000 detectors, equipped with graphite monochromated Mo Kalpha radiation (= 0.71073 Å) at 293K. The 2 $\theta$  range for data collection

was from 5.082 to 50. The data interpretation was processed with CrysAlisPro, Xtlab Synergy Rigaku oxford diffraction, version 171.39.exe and an absorption correction based on the multi-scan method.

**TEM images:** TEM images are recorded using a JEM-F200 kV. The sample preparation was done by taking the powder on the Cu grid. The TEM photo is analyzed by Gatan Digital Micrograph software.

**SCLC measurements:** I-V curves have been measured using the solar simulator and Keithley 2400 at 25 °C in ambient conditions.

The microcrystalline strain was calculated using Williamson-Hall (W-H) plots (Equation 1) from powder XRD data.

$$\beta_{hkl} \cos\theta = \frac{K\lambda}{D} + 4\varepsilon \sin\theta \quad (1)$$

Where D = crystalline size, K = shape factor (0.9), and  $\lambda$  = wavelength of  $\text{Cu}\alpha$  radiation, instrumental broadening ( $\beta_{hkl}$ ). The strain  $\varepsilon$  was estimated from the slope of Equation 1 (Supporting information **Fig. S3(b)**).

### 1.3. Experimental details of Terahertz time-domain spectroscopy (THz-TDS)

We have built the THz-TDS system in the 0.1 to 3.0 THz range. The setup consists of a Ti:Sapphire laser (800 nm, 35 fs, 1 kHz). A beam splitter (90:10) was used to split the output beam into pump (generation arm) and probe (detection arm) sources. We have fixed the pump's laser pulse energy at 1.5 mJ and 3  $\mu\text{J}$  for probe pulses. The pump and probe pulses were focused by a spherical lens of 150 mm (beam waist ( $\omega_0$ ) = 16.5  $\mu\text{m}$ ) and 300 mm ( $\omega_0$  = 30.75  $\mu\text{m}$ ) focal lengths.

A 200  $\mu\text{m}$  thick type 1 BBO crystal was used to convert the fundamental 800 nm to second harmonic 400 nm wavelength and placed between the spherical lens and its focus position. The generated THz radiation from air plasma was guided by four gold-coated half-axis parabolic mirrors (PM) until the THz signal was focused on the ZnTe (110) crystal (EKSMA optics) having a 1 mm thickness. For the SCs THz reflection and transmission measurements, the SCs are positioned at  $0^\circ$  and  $45^\circ$  to the incident THz pulse. The THz pulse reflection from single crystals was collected by PM5 and guided with a gold-coated mirror. In the case of transmission, this mirror was flipped down. THz radiation was detected using an electro-optical sampling technique consisting of ZnTe crystal, quarter waveplate, Wollaston prism, and balanced photodiodes. The residual input laser was blocked by high resistivity float zone silicon (HRFZ-Si) after the PM1. The output of the balanced diode signal was connected to the lock-in amplifier (Stanford Research Systems, model no. SR830). The pump pulse is chopped at 500 Hz using a mechanical optical chopper as a reference to the lock-in amplifier. The LabVIEW program controlled the delay stage's data acquisition and motion control.

**1.4. HHG experimental setup:** The schematic used for HHG measurements was earlier reported.<sup>3,4</sup> In brief, we used a Ti: Sapphire laser (800 nm, 35 fs) operated at a 1 kHz pulse repetition rate used as a DP. Used picoseconds (800 nm, 200 ps, 1 kHz) and nanoseconds (1064 nm, 5ns, 10 Hz) HP to create the plasma plumes of SCs. The picoseconds pulses are obtained from an uncompressed portion of amplified laser pulses of the same Ti: Sapphire laser system. The delay between the fs DP and ps HP was fixed at approximately 80 ns. In contrast, the delay dependence between ns HP and fs DP was varied using the digital delay line and controlled by a delay generator (DG535, Stanford Research Systems). The DPs and HPs are focused using a spherical lens of 500 mm and 200 mm, respectively. In case of ps HPs the HHG studies were carried out at (a) different

DP intensities between  $1.5$  to  $9 \times 10^{14}$  W/cm<sup>2</sup> at fixed ps HP intensity  $1.17 \times 10^{10}$  W/cm<sup>2</sup> and (b) ps HP intensities are varied from  $0.6$  to  $2.25 \times 10^{10}$  W/cm<sup>2</sup> at fixed DP intensity  $6.0 \times 10^{14}$  W/cm<sup>2</sup>. In the case of ns HP its intensity was fixed at  $7 \times 10^{10}$  W/cm<sup>2</sup>. The synthesized SCs are placed on a glass substrate and kept perpendicular to the HP propagation in the target chamber. The DPs propagated through the plasma plumes approximately  $0.2$  mm above the target surface. The emitted harmonics from LIPs were directed to the XUV spectrometer chamber, consisting of a gold-coated cylindrical mirror, flat field grating, and a microchannel plate. The harmonic spectra were recorded using a charge-coupled device camera.

**Table S1:** Literature review

Year	Growth Method	Additives used	Perovskite material used	Application	Ref
2016	ITC	–	CH <sub>3</sub> NH <sub>3</sub> PbI <sub>3</sub> (Cl)	Optoelectronic Devices	5
2016	–	–	CH <sub>3</sub> NH <sub>3</sub> PbI <sub>3</sub> single crystals.	–	6
2017	ITC	–	(FAPbI <sub>3</sub> ; FA <sup>+</sup> = HC(NH <sub>2</sub> ) <sub>2</sub> <sup>+</sup> ) single crystals	–	7
2018	AVC	–	MAPbX <sub>3</sub>	Alpha Source	8
2019	AVC	–	CsPbBr <sub>3</sub> microrod Single Crystals	High Detectivity Photodetectors	9
2019	ITC	–	MAPbBr <sub>3-x</sub> Cl <sub>x</sub> (MH)	Scintillation	10
2020	ITC	–	MAPbBr <sub>3-x</sub> Cl <sub>x</sub> (MH)	–	11
2020	ITC	–	MAPb(Br <sub>1-x</sub> Cl <sub>x</sub> ) <sub>3</sub>	Electrical Properties	12
2020	ITC	Choline Bromide (CB)	CsPbBr <sub>3</sub> Single Crystals	γ-Ray Response	13
2020	ITC	–	MH-3D-Single Crystals	Cr/MAPbBr <sub>3-x</sub> Cl <sub>x</sub> /Cr Γ-Ray Responses.	14
2021	ITC	Polymer	FAPbI <sub>3</sub> , MAPbI <sub>3</sub> , MAPbBr <sub>3</sub> , and	–	15

FAPbBr <sub>3</sub>					
2021	Spin-Coated	2-(2-(2-Aminoethoxy)ethoxy)acetic acid,	FAPbI <sub>3</sub> -Film	Perovskite LEDs	<sup>16</sup>
2021	Bridgman crystal growth method	–	CsPbBr <sub>3</sub> Single Crystals	Γ-Ray Response	<sup>17</sup>
2022	ITC	Polymer	MAPbI <sub>3</sub>	Photodetection	<sup>18</sup>
2022	ITC	<b>Chiral and non-Chiral additives</b>	<b>MAPbBr<sub>3</sub></b>	<b>THz and HHG</b>	<b>This work</b>

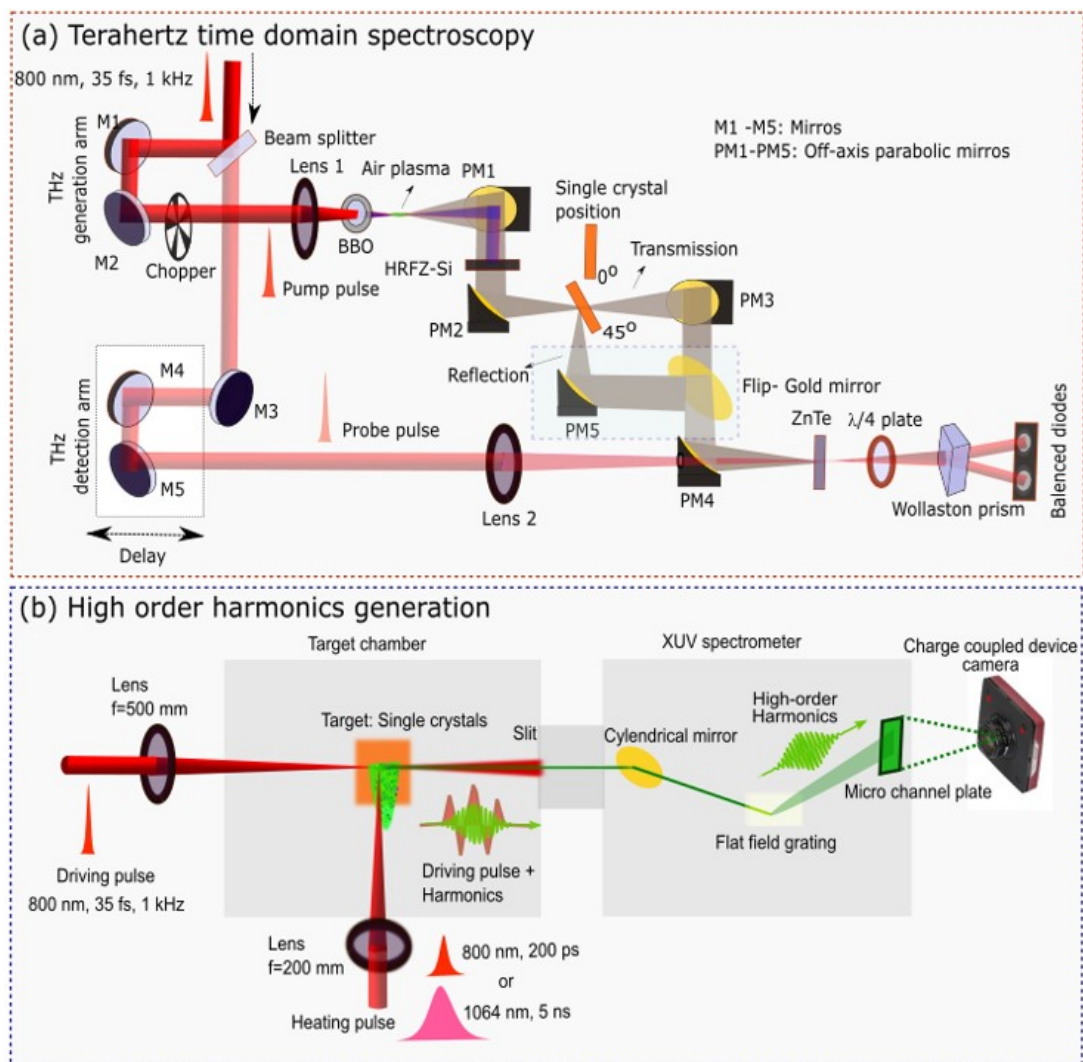


**Fig. S1.** Experimental layout for (a) terahertz time-domain spectroscopy and (b) high-order harmonics from laser-induced plasma plumes of single perovskite crystals.

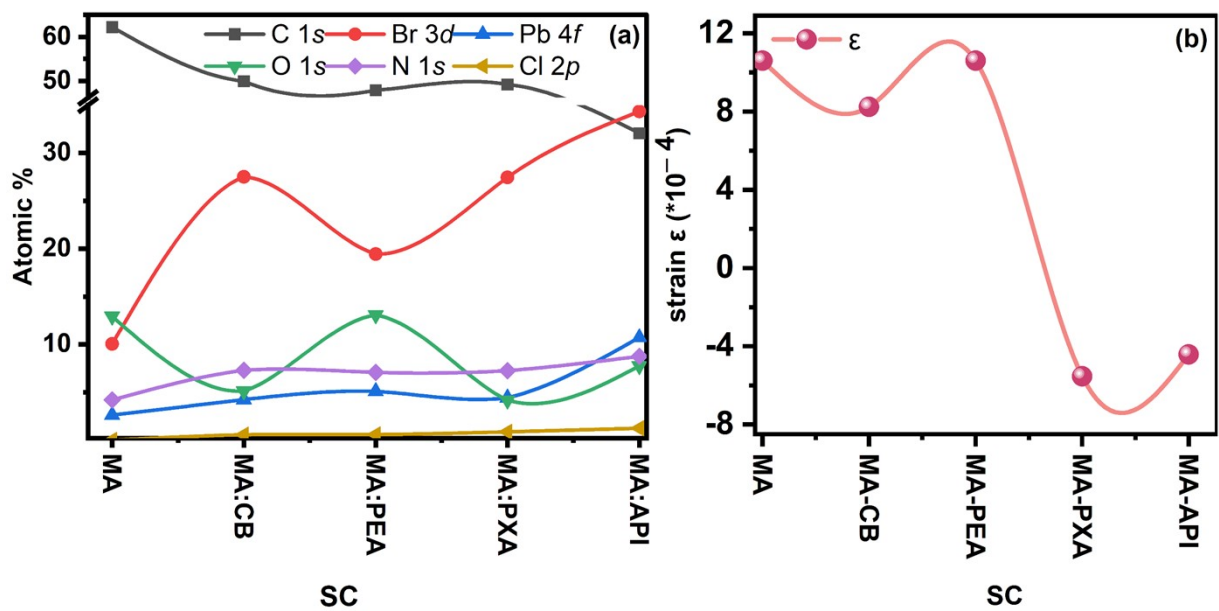


**Fig. S2.** (a) Atomic Ratio of MAPbBr<sub>3</sub> perovskite single crystal with changing additives. (b) Lattice strain values of each reported crystal were calculated from the W-H plot using the XRD data.

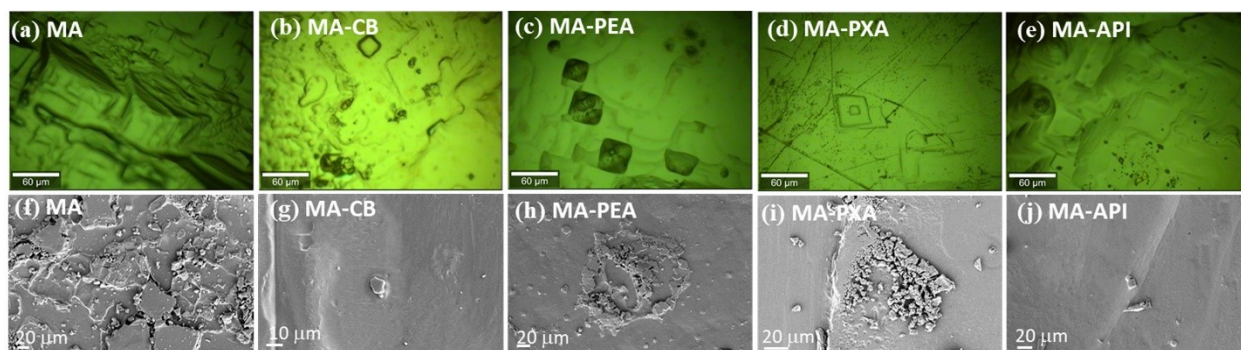


**Fig. S3.** (a-e) Confocal and (f-j) scanning electron microscopy (SEM) images of MA crystals grown using the additives corresponding to CB, PEA, PXA, and API samples, respectively.

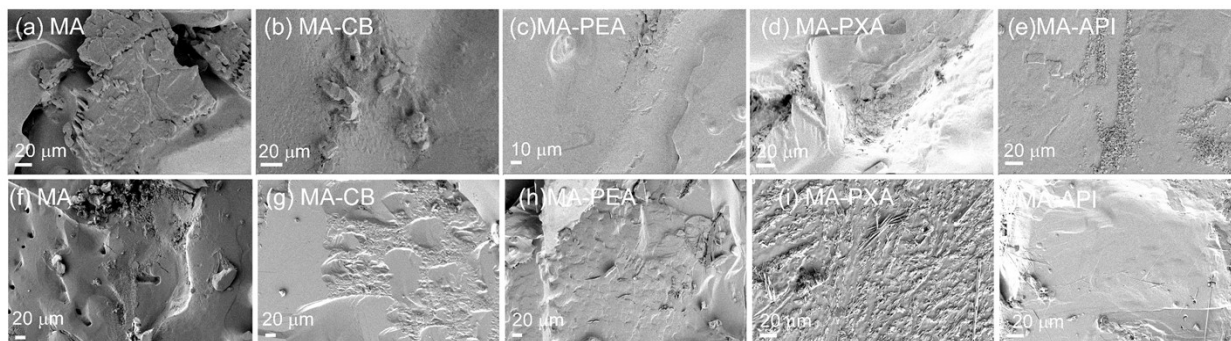


**Fig. S4.** (a)-(e) SEM images taken after keeping PSCs in ambient conditions for three and (f-j) seven days, respectively.

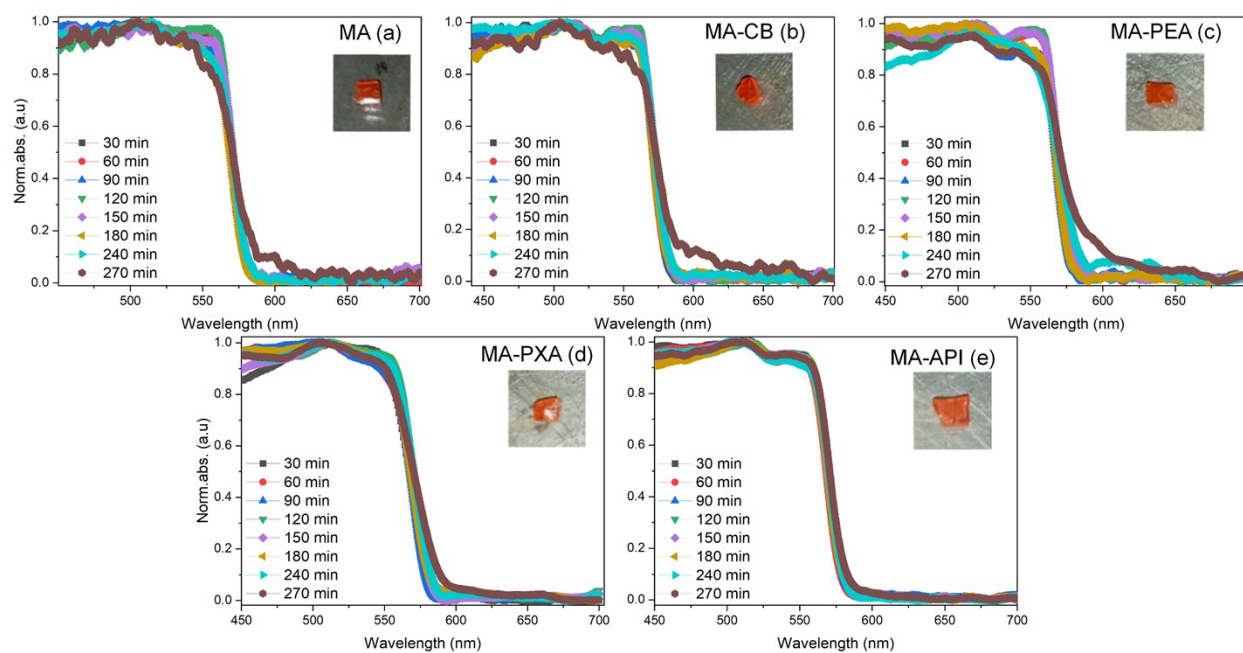


**Fig. S5.** (a)-(e) Surface degradation of SCs in the outer atmosphere at a constant temperature at different time intervals were studied using UV spectroscopy.

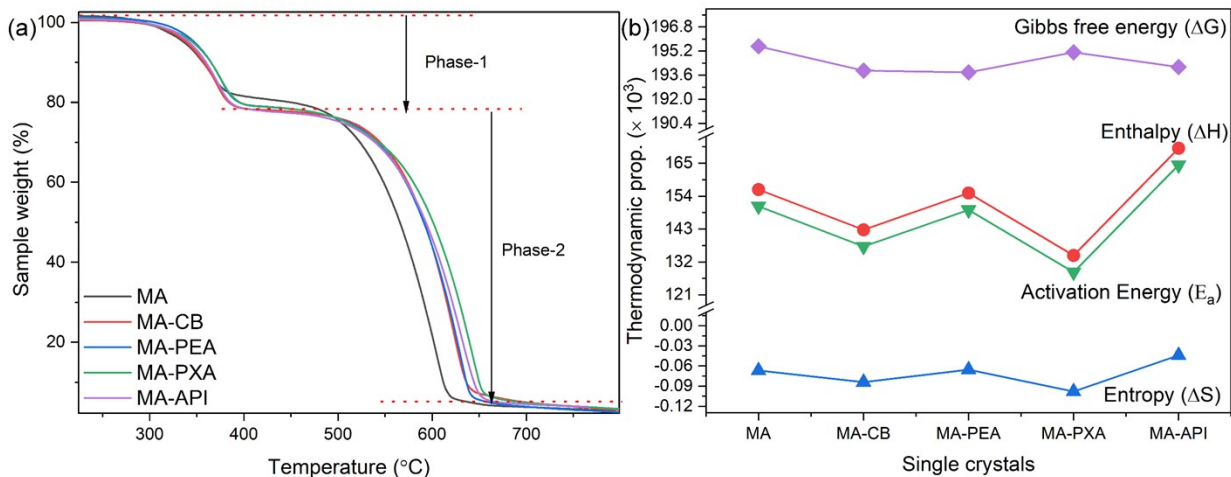


**Fig. S6.** (a)-(b) Comparative Study of MHPSCs Thermogravimetric Analysis (TGA), and thermodynamic properties of phase one (P1- Organic part decomposition) for all the crystals.

**Table. S2.** Crystal data and structure refinement for MA and modified PSCs.

Single crystals	Initial temperature (K)	Activation energy Ea (kJ mol <sup>-1</sup> )	Entropy change ΔS (J/g K)	Enthalpy change ΔH (kJ/g)	Gibbs free energy ΔG (kJ mol <sup>-1</sup> )
MA	225	156.22	-66.69	150.63	195.52
MA-CB	231	142.77	-84.063	137.16	193.91
MA-PEA	230	155.05	-65.44	149.41	193.79
MA-PXA	224	134.20	-98.16	128.57	195.12
MA-API	232	170.03	-44.032	164.42	194.14

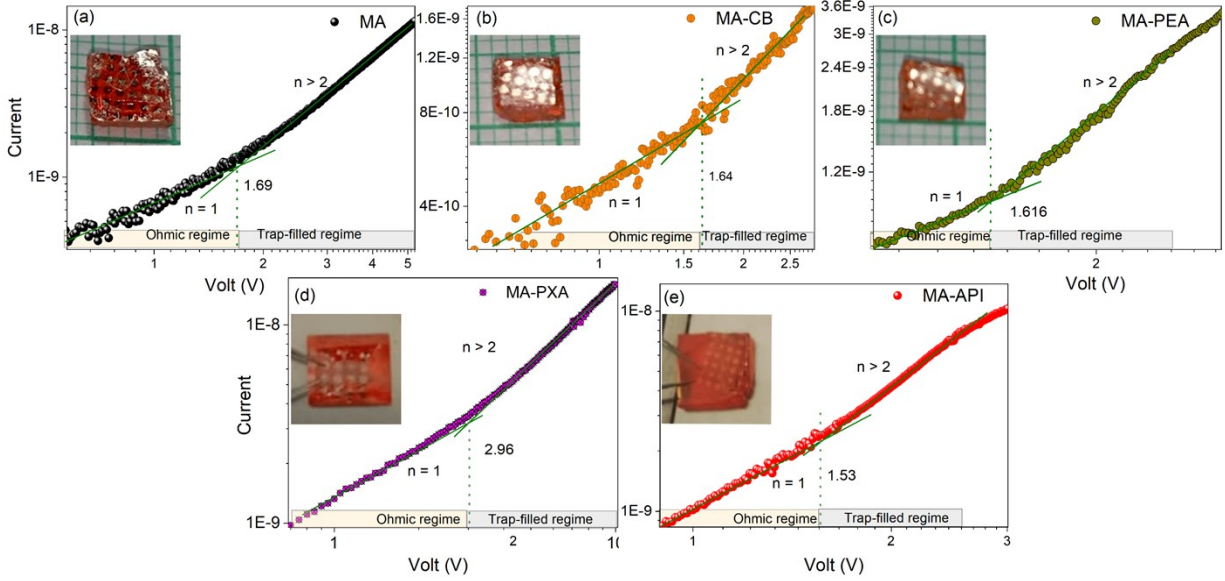


**Fig. S7.** (a)-(e) Fig. S7(a)-(e) Current-voltage traces with insert showing SCs deposited with Au. The linear fitting is denoted with the green markers showing different regimes (at 300 K).

**Table. S3** Crystal data and structure refinement for MA and modified PSCs.

Parameters	MA	MA-CB	MA-PEA	MA-PXA	MA-API
Temperature	296(2) K	293(2) K	293(2) K	295(2) K	299(2) K
Wavelength	71.073 pm				
Crystal system	Cubic	Cubic	Cubic	Cubic	Cubic
Space group	P m -3 m	P -4 3 m	P m -3 m	P m -3 m	P m -3 m
Unit cell dimensions	$a = b = c = 5.9 \text{ \AA}$ $\alpha = \beta = \gamma = 90^\circ$	$a = b = c = 5.8 \text{ \AA}$ $\alpha = \beta = \gamma = 90^\circ$	$a = b = c = 5.9 \text{ \AA}$ $\alpha = \beta = \gamma = 90^\circ$	$a = b = c = 5.9 \text{ \AA}$ $\alpha = \beta = \gamma = 90^\circ$	$a = b = c = 5.9 \text{ \AA}$ $\alpha = \beta = \gamma = 90^\circ$
Volume	0.207885 nm <sup>3</sup>	0.20413 nm <sup>3</sup>	0.2073 nm <sup>3</sup>	0.20783 nm <sup>3</sup>	0.20712 nm <sup>3</sup>
Z	1	3	1	1	1
Density (calculated)	5.984 mg/m <sup>3</sup>	4.319 mg/ m <sup>3</sup>	3.789 mg/ m <sup>3</sup>	4.346 mg/ m <sup>3</sup>	4.257 mg/ m <sup>3</sup>
Absorption	34.73 mm <sup>-1</sup>	35.28 mm <sup>-1</sup>	34.70 mm <sup>-1</sup>	34.66 mm <sup>-1</sup>	34.77 mm <sup>-1</sup>

<b>coefficient</b>					
<b>F(000)</b>	338	229	200	236	229
<b>Crystal size</b>	0.240 x 0.200 x 0.190 mm <sup>3</sup>	0.24 x 0.14 x 0.21 mm <sup>3</sup>	0.250 x 0.230 x 0.170 mm <sup>3</sup>	0.210 x 0.200 x 0.170 mm <sup>3</sup>	0.200 x 0.190 x 0.140 mm <sup>3</sup>
<b>Theta range for data collection</b>	3.439 to 26.930°	3.457 to 26.858°	3.439 to 27.508°	3.439 to 26.676°	3.443 to 26.966°
<b>Index ranges</b>	-7<=h<=7, - 7<=k<=7, - 7<=l<=7	-6<=h<=7, - 7<=k<=6, - 7<=l<=5	-7<=h<=7, - 7<=k<=7, - 7<=l<=7	-7<=h<=7, - 4<=k<=4, - 7<=l<=4	-7<=h<=7, - 7<=k<=6, - 7<=l<=7
<b>Reflections collected</b>	4933	787	1794	507	1500
<b>Independent reflections</b>	70 [R(int) = 0.4355]	107 [R(int) = 0.9681]	74 [R(int) = 0.5778]	69 [R(int) = 0.4153]	70 [R(int) = 0.5472]
<b>Completeness to <math>\theta = 25.242^\circ</math></b>	100.0 %	98.2 %	100.0 %	100.0 %	100.0 %
<b>Refinement method</b>	Full-matrix least-squares on F2	Full-matrix least-squares on F2	Full-matrix least-squares on F2	Full-matrix least-squares on F2	Full-matrix least-squares on F2
<b>Data / restraints / parameters</b>	70 / 0 / 9	107 / 0 / 8	74 / 0 / 8	69 / 0 / 5	70 / 0 / 5

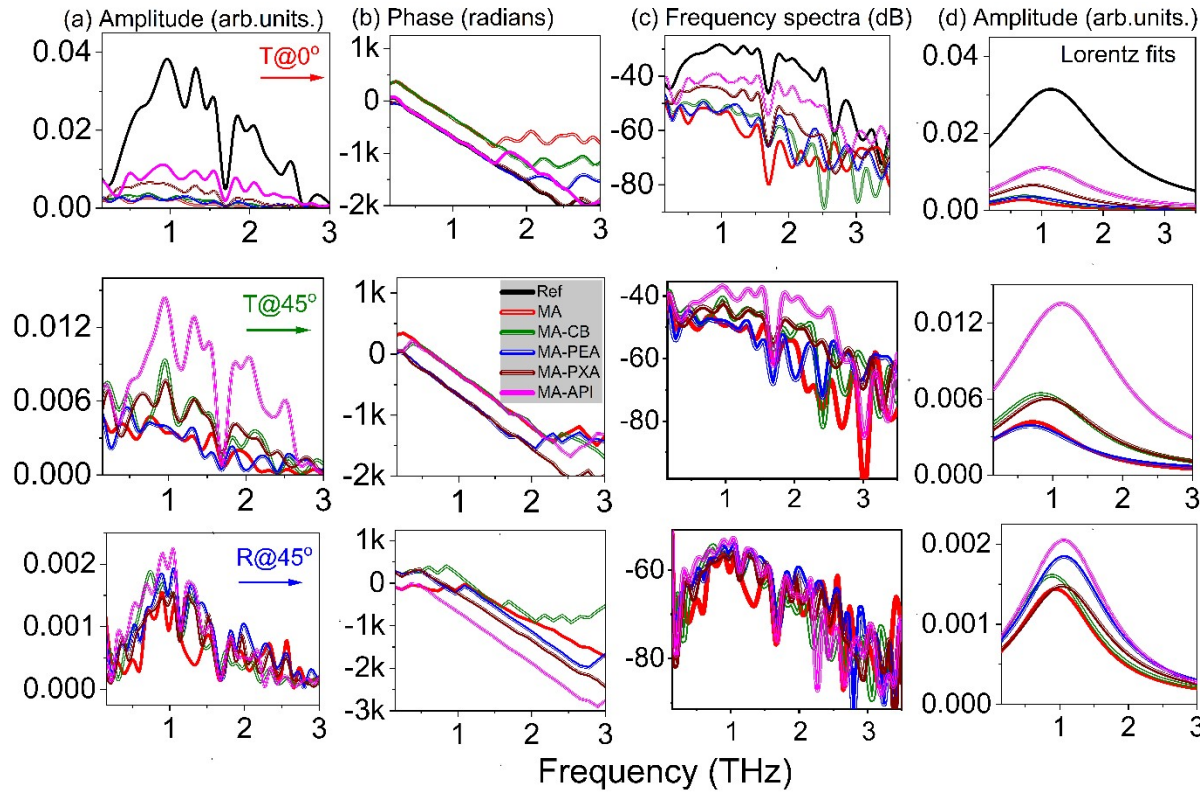


**Fig. S8.** After the conversion of the THz electric field to FFT spectra, the obtained (a) THz amplitude, (b) phase, (c) frequency spectra in dB, (d) Lorents fits of data points from THz amplitude shown in (a), for transmittance (T) @  $0^\circ$ , (upper row), T@  $45^\circ$  (middle row), reflection @  $45^\circ$  from reference and perovskite single crystals, respectively. The legend is shown in (b, middle panel), applicable to all panels; Black: solid line, red: solid line, green: double line, blue: thick-thin line, wine: thin-thick line, and magenta: triple lines corresponding to reference pulse, for Singles crystals MA, MA-CB, MA-PEA, MA-PXA and MA-API. The Y-axis labels are shown on top of each column after the figure labels (a),(b),(c) and (d).

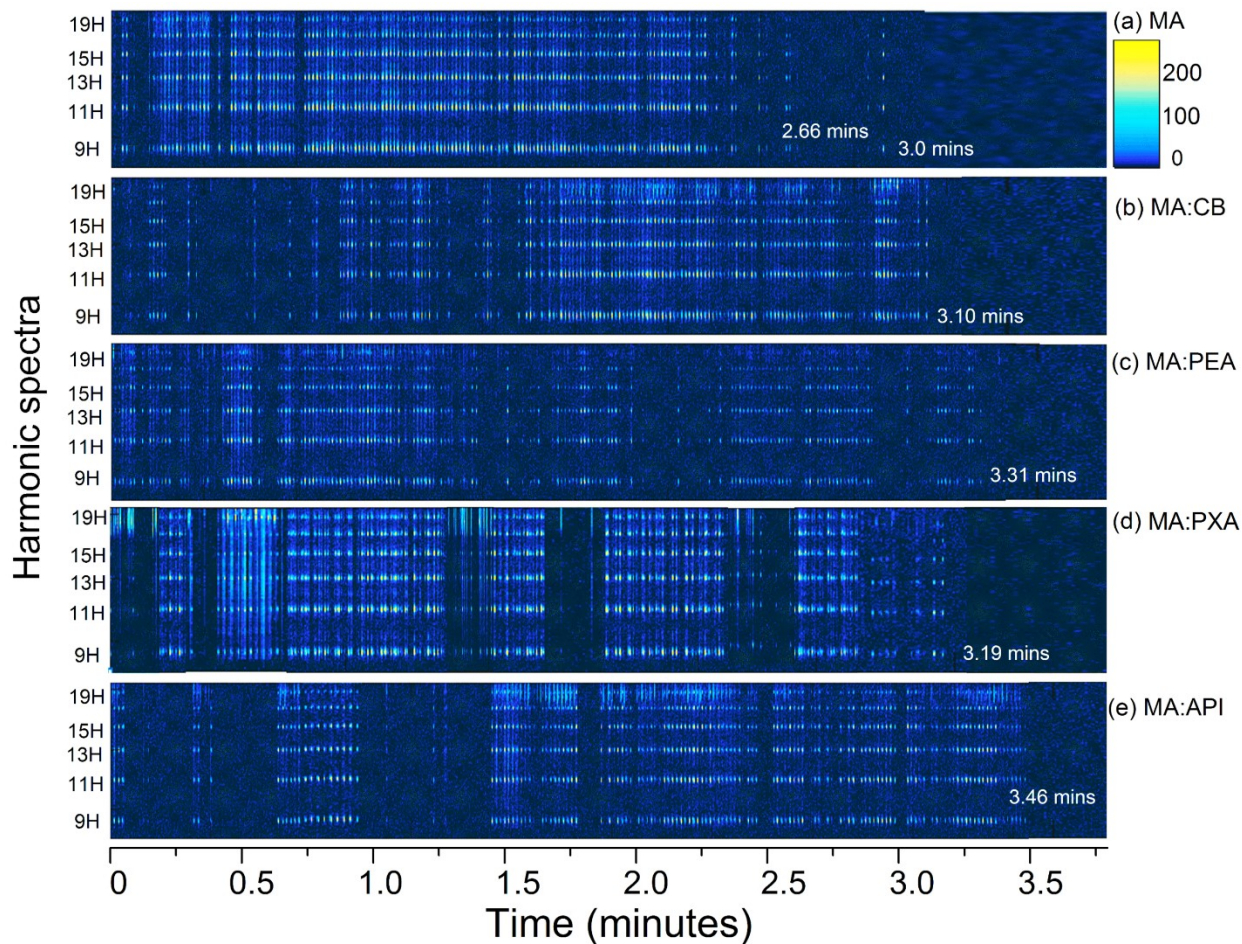


**Fig. S9.** (a)-(e) The vertical representation of harmonic spectra of SCs. The spectra were recorded for time duration. The plasma plumes are produced by nanoseconds heating pulses at a fixed position on the surface of SCs.

**Table. S4** First and second ionization potentials for chemical elements present in single crystals.

Single crystal	Molecular formula	Elements	Ionization potential (eV)	
			I	II
MA	CH <sub>3</sub> NH <sub>3</sub> PbBr <sub>3</sub>	C	11.26	24.38
		H	13.59	-
		N	14.53	29.60

		Pb	7.41	15.03
		Br	11.81	21.80
MA-CB	CH <sub>3</sub> NH <sub>3</sub> PbBr <sub>3</sub> :C <sub>5</sub> H <sub>14</sub> BrNO	O	13.61	35.11
MA-PEA	CH <sub>3</sub> NH <sub>3</sub> PbBr <sub>3</sub> :C <sub>8</sub> H <sub>12</sub> ClN	Cl	12.96	23.81
MA-PXA	CH <sub>3</sub> NH <sub>3</sub> PbBr <sub>3</sub> :C <sub>8</sub> H <sub>14</sub> Cl <sub>2</sub> N <sub>2</sub>	*		
MA-API	CH <sub>3</sub> NH <sub>3</sub> PbBr <sub>3</sub> :C <sub>5</sub> H <sub>14</sub> Cl <sub>2</sub> N <sub>2</sub>	*		

## REFERENCES

- 1 Y. Liu, Z. Yang, D. Cui, X. Ren, J. Sun, X. Liu, J. Zhang, Q. Wei, H. Fan, F. Yu, X. Zhang, C. Zhao and S. Liu, *Advanced Materials*, 2015, **27**, 5176–5183.
- 2 M. Ng and J. E. Halpert, *RSC Advances*, 2020, **10**, 3832–3836.
- 3 S. R. Konda, V. R. Soma, M. Banavoth, R. Ketavath, V. Mottamchetty, Y. H. Lai and W. Li, *ACS Applied Nano Materials*, 2021, **4**, 8292–8301.
- 4 S. R. Konda, Y. H. Lai and W. Li, *Journal of Applied Physics*, 2021, **130**, 013101.
- 5 Z. Lian, Q. Yan, T. Gao, J. Ding, Q. Lv, C. Ning, Q. Li and J. L. Sun, *Journal of the American Chemical Society*, 2016, **138**, 9409–9412.
- 6 R. Ketavath, N. K. Katturi, S. G. Ghugal, H. K. Kolli, T. Swetha, V. R. Soma and B. Murali, *The Journal of Physical Chemistry Letters*, 2019, **10**, 5577–5584.
- 7 T. Sekimoto, M. Suzuka, T. Yokoyama, R. Uchida, S. Machida, T. Sekiguchi and K. Kawano, *Physical Chemistry Chemical Physics*, 2018, **20**, 1373–1380.

- 8 H. Shen, *Journal of Materials Science*, 2019, **54**, 11596–11603.
- 9 X. Cheng, Y. Yuan, L. Jing, T. Zhou, Z. Li, Z. Peng, Q. Yao, J. Zhang and J. Ding, *Journal of Materials Chemistry C*, 2019, **7**, 14188–14197.
- 10 Y. Li, W. Shao, X. Ouyang, X. Ouyang, Z. Zhu, H. Zhang, B. Liu and Q. Xu, *Journal of Physical Chemistry C*, 2019, **123**, 17449–17453.
- 11 L. T. Mix, D. Ghosh, J. Tisdale, M.-C. Lee, K. R. O’Neal, N. Sirica, A. J. Neukirch, W. Nie, A. J. Taylor, R. P. Prasankumar, S. Tretiak and D. A. Yarotski, *The Journal of Physical Chemistry Letters*, 2020, **11**, 8430–8436.
- 12 L. Qiu, Z. Wang, S. Luo, C. Li, L. Wang, S. Ke and L. Shu, *Journal of Crystal Growth*, 2020, **549**, 125869.
- 13 Y. Feng, L. Pan, H. Wei, Y. Liu, Z. Ni, J. Zhao, P. N. Rudd, L. R. Cao and J. Huang, *Journal of Materials Chemistry C*, 2020, **8**, 11360–11368.
- 14 N. Rybin, D. Ghosh, J. Tisdale, S. Shrestha, M. Yoho, D. Vo, J. Even, C. Katan, W. Nie, A. J. Neukirch and S. Tretiak, *Chemistry of Materials*, 2020, **32**, 1854–1863.
- 15 L. Ma, Z. Yan, X. Zhou, Y. Pi, Y. Du, J. Huang, K. Wang, K. Wu, C. Zhuang and X. Han, *Nature Communications*, 2021, **12**, 2023.
- 16 L. Zhu, H. Cao, C. Xue, H. Zhang, M. Qin, J. Wang, K. Wen, Z. Fu, T. Jiang, L. Xu, Y. Zhang, Y. Cao, C. Tu, J. Zhang, D. Liu, G. Zhang, D. Kong, N. Fan, G. Li, C. Yi, Q. Peng, J. Chang, X. Lu, N. Wang, W. Huang and J. Wang, *Nature Communications*, 2021, **12**, 5081.

- 17 Y. He, M. Petryk, Z. Liu, D. G. Chica, I. Hadar, C. Leak, W. Ke, I. Spanopoulos, W. Lin, D. Y. Chung, B. W. Wessels, Z. He and M. G. Kanatzidis, *Nature Photonics*, 2021, **15**, 36–42.
- 18 N. Parikh, P. Sevak, S. Jowhar Khanam, D. Prochowicz, S. Akin, S. Satapathi, M. M. Tavakoli, M. Banavoth, A. Kalam and P. Yadav, *ACS Omega*, 2022, **7**, 36535–36542.